Journal of
Nanoscience and Nanotechnology
Vol. 6, 2103–2109, 2006

RESEARCH ARTICLE

Synthesis and Characterisation of YSZ–Al_2O_3 Nanostructured Materials

J. Santoyo-Salazar[1,*], G. González[1], P. S. Schabes-Retchkiman[2], J. A. Ascencio[3], J. Tartaj-Salvador[4], and J. A. Chávez-Carvayar[1]

[1] *Instituto de Investigaciones en Materiales, UNAM, Circuito Exterior s/n. C. U. A. Postal 70-360, C. P. 04510, México, D. F. México*
[2] *Instituto de Física, UNAM, A. Postal 20-364, C. P. 01000, México, D. F. México*
[3] *Instituto Mexicano del Petróleo, Eje Central Lázaro Cárdenas 152, San Bartolo Atepehuacan, C. P. 07730, México, D. F. México*
[4] *Instituto de Cerámica y Vidrio, CSIC, Campus Cantoblanco, C/ Sor Juana Inés de la Cruz s/n. 28049, Madrid, España*

In this work a co-precipitation route was used to synthesise two yttria-stabilised-zirconia (YSZ) phases with different concentrations of alumina (Al_2O_3). A tetragonal, with 3 mol% yttria, and a cubic, with 8 mol% yttria, phases were added with alumina in different weight proportions, 90/10, 80/20, 70/30, and 60/40, respectively. After synthesised, products were sintered in a range 800–1100 °C for different intervals of time. Compounds were characterised by X-ray diffraction, transmission electron microscopy (TEM), high resolution transmission electron microscopy (HRTEM), scanning electron microscopy (SEM), and atomic force microscopy (AFM). Rietveld refinements, using FULPROF-Suite software, were carried out to obtain the cell parameters and structural characterisation of products.

Keywords: Yttria-Stabilised-Zirconia, Co-Precipitation, Nanocompound, High Resolution Microscopy, Rietveld Refinement.

1. INTRODUCTION

Development of new functional materials is based on the improvement of synthesis methods and the knowledge of the produced structures, besides the understanding of those variables with a special meaning in the physical properties of the material. In the area of functional ceramics, recently, the tendency to stabilise zirconia (ZrO_2) has grown, reaching this material a remarkable technological importance due to its high ionic conductivity at elevated temperature, which can be applied to produce solid electrolytes for solid oxide fuel cells (SOFC),[1–5] oxygen gas sensors and oxygen membrane separator.[6,7] However, the strength,[8] thermal and chemical stability of ZrO_2 must be improved during the material performance.[9,10]

Stable structures of tetragonal, t-ZrO_2, or cubic, c-ZrO_2, zirconia can be obtained by replacing zirconium atoms by cations with lower charge, producing oxygen vacancies through the lattice. Under these conditions ion conductivity can be observed, in a temperature range 600 to 1000 °C, on these structures.[11,12] Zirconia can be stabilised by appropriate additions of metallic oxides of the type MO, MO_2, and M_2O_3. These substitutions have demonstrated to be an excellent way to generate superficial active sites as well, which are fundamental for catalysis and electrolytes.[13,14] Addition of oxides like MgO, CaO, CeO_2, Sc_2O_3, Y_2O_3, and Al_2O_3 also can induce structural stability and produce vacancies in ZrO_2.[15]

Although yttria (Y_2O_3) is mainly used to stabilise zirconia, under operating conditions, produced electrolytes may exhibit some problems due to phase transformations, decreasing the ionic conductivity and deteriorating the mechanical properties of yttria-stabilised-zirconia (YSZ); and if it is applied to a solid oxide fuel cells (SOFC) the efficiency of this device is reduced. Therefore, YSZ electrolytes must have high stability, density, and reproducibility of their physical properties with increasing temperature.[16–18]

Alumina (Al_2O_3) is another M_2O_3 oxide with good properties such as high mechanical strength and stability at high temperature, which can be added to YSZ because of the lower valence of Al (3+) compared to (4+) of Zr. The ionic size radius of Al^{3+} (0.53 Å) is too small to substitute Zr^{4+} (0.84 Å) and to be coordinated with eight oxide ions in tetragonal and cubic ZrO_2[19] so that, a soft synthesis route is suggested to incorporate Al^{3+} to YSZ. Therefore, it is important to have a homogenous dispersion of YSZ–Al_2O_3, otherwise, high concentration or a

*Author to whom correspondence should be addressed.

 1533-4880/2006/6/2103/007 doi:10.1166/jnn.2006.334

non-homogenous dispersion of alumina would reduce the mechanical and ion conductivity properties of ZrO_2.[20]

Among the different routes to synthesise ceramic materials with nanometric particle size such as sol–gel,[21] combustion,[22] polymerisation,[23] and co-precipitation,[24] in this work, the co-precipitation route was used to stabilise *t*-YSZ and *c*-YSZ with a controlled dispersion of powder in reactive solutions, making possible the homogeneous distribution and consequently, the inclusion of alumina in the YSZ lattices. Besides, nanometric particle sizes can be obtained at low temperatures.

Addition of Al_2O_3 in YSZ has been reported with proportions of 30, 25, and 20 wt% increasing the mechanical strength of products; however the particle size of Al_2O_3 affected its distribution in the sintered material.[26–29] In this work, microstructural and morphological properties of *t*-YSZ (3 mol% YSZ) and *c*-YSZ (8 mol% YSZ), which were doped with 10–40 wt% of Al_2O_3 and sintered in the temperature range of 800–1000 °C, are presented.

Because of the importance of the structure for the searched properties, the use of detailed crystallographic and morphological analyses were used to study the obtained material. The crystallographic phase identification was analysed by X-ray diffraction; while the use of scanning electron microscopy (SEM) and atomic force microscopy (AFM) allowed to observe the nanometric domains of the aggregates; these techniques gave the 2D and 3D understanding that is required for technological applications at the macroscopic scale.[13, 30] Finally the particle size distribution and the internal structure, of *t*-YSZ and *c*-YSZ doped with Al_2O_3 were studied by transmission electron microscopy (TEM) and high resolution transmission electron microscopy (HRTEM).

2. EXPERIMENTAL DETAILS

2.1. Preparation

Tetragonal, *t*-YSZ/Al_2O_3, powders with 90/10, 80/20, 70/30, and 60/40 wt% of (3 mol% YSZ)/Al_2O_3 proportions, were prepared by the co-precipitation route. Starting precursor Al_2O_3 was obtained by mixing aluminium nitride ($Al(NO_3)_3 \cdot 9H_2O$) in ionised water. Crystalline particles of Tosoh 3 mol% yttria stabilised zirconia were suspended in ionised water and added into the transparent dissolution of $Al(NO_3)_3 \cdot 9H_2O$, in proportions of 10, 20, 30, and 40 wt% Al_2O_3. To precipitate the Al^{3+}, NH_4OH was diluted at 50% with the precursor solution, pH = 9, with constant stirring in all the process. After the reaction, samples were washed with deionised water and pure ethanol to reduce the remaining water amount and capillarity between particles. Powders were dried at 90 °C, then grounded and fired at 300 °C for 20 h. In addition, *c*-YSZ based compounds were prepared with concentrations of 90/10, 80/20, 70/30, and 60/40 wt% of (8 mol% YSZ)/Al_2O_3. These compounds were produced

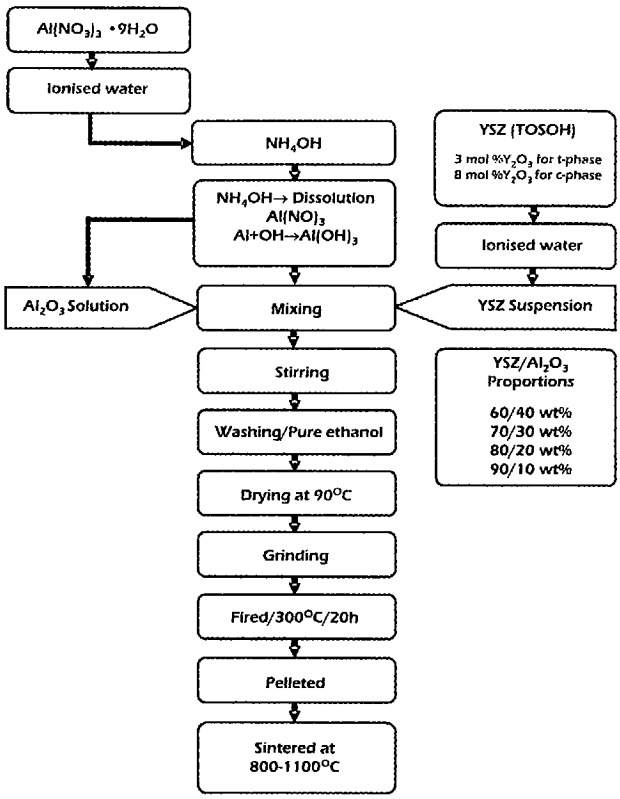

Fig. 1. Flow chart of the co-precipitation route to obtain (3 and 8 mol% YSZ)/Al_2O_3 compounds.

with a similar starting Al_2O_3 precursor $Al(NO_3)_3 \cdot 9H_2O$ and Tosoh 8 mol% yttrium stabilised zirconia under the same conditions than (3 mol% YSZ)/Al_2O_3 powders, the flow chart for these processes are shown in Figure 1. Finally, for both series of compounds, samples of 0.2 g were pelleted to 13 mm diameter and 0.5 mm thickness under a 150 MPa. Pellets were sintered in a range of 800–1100 °C for 2, 6, and 15 h to identify structural changes in YSZ/Al_2O_3.

2.2. Characterisation

Phase identification of samples was carried out with a Bruker AXS, D8 Advanced, X-ray diffractometer, with monochromatic Cu$k\alpha$ radiation, $\lambda = 1.54056$ Å, with 35 kV and 30 mA. Scanning steps of 0.02 2θ degrees were used in the range 20–90° with 2 sec/step. For accurate determination of lattice parameters and for structural studies of the new phase, the scanned range was 10 to 120° 2θ, with a step of 0.02° 2θ and 10 seconds/step.

Results were analysed with Diffrac Plus Software and compared to JCPDF standards. Lattice parameters and peak identification of a novel *t*-YSZ were obtained by Rietveld refinement using FULPROF-Suite software (release July 2004). Background was approximated by a linear interpolation between 70 data points. For the peak shape, a Thompson–Cox–Hastings pseudo–Voigt profile

function was used. Instrumental profile was based on LaB_6 results and then it was incorporated to the refinement. In a similar way, the cubic phase, *c*-YSZ, was also indexed and refined.

For superficial studies, a Leica-Cambridge Stereoscan 440 SEM, was used to analyse the morphology, distribution, and grain size of the materials. Operating conditions were 20 kV, 300–750 pA, and WD 9–12 mm, with a QBSD detector. Samples were coated with a thin gold film, which was obtained with a sputtering JEOL ion coating system at 0.5 kV and 11 mA. An Oxford ISIS energy dispersive spectroscopy (EDS) device linked to the SEM was used to obtain the elemental composition of the samples. To analyse the topography, profiles, and particle size, a JEOL JSPM-4212 Scanning Probe Microscope, was used with the Tapping mode under normal pressure conditions, with CSC 21/25–NSC 15/25 Ultra-Sharp silicon cantilevers, at different RMS conditions. Transmission electron microscopy studies were carried out with a JEM1200EX, at 100 keV and a JEM2010FEG at 200 keV equipped with a field emission gun for high resolution TEM and also with a high-angle-annular-dark-field (HAADF) detector in the STEM mode to obtain *Z*-contrast like micrographs.[32] Samples were prepared from dispersed powders on a 300 mesh copper grids. High resolution was obtained under the optimum conditions of contrast and focus based on the Scherzer parameters. Electron energy loss spectroscopy (EELS) was also carried out to identify the elemental species in the observed regions of the samples. To increase the symmetry details, the fast Fourier transform (FFT) spectra were digitally obtained from the HRTEM images.

3. RESULTS AND DISCUSSION

3.1. Structural Analysis

A first series of samples were obtained with *t*-YSZ/Al_2O_3. XRD analysis revealed that temperature, sintering time, and Al_2O_3 concentration introduce some structural changes, in 60/40 wt% proportions there were some diffracted peaks which correspond to the monoclinic phase of zirconia, although the sintering time and temperature were modified the monoclinic diffraction peaks were present. On the other hand, by reducing Al_2O_3 concentration to 10 wt%, a tetragonal *t*-ZrO_2 based phase was present at different temperatures and sintering times, Figure 2.

Although the addition of Al_2O_3 in the tetragonal zirconia phase did not change the structure of new products, as it was observed in the XRD patterns, there was a small shift in the 2θ peak positions leading the cell parameters and space group to $a = 5.09964$ Å, $c = 5.17488$ Å, and *P42/ncm*, which may be associated to the replacement of Zr^{4+} by Y^{3+} or Al^{3+} (Ref. [32]). Chemistry defect substitution relations can be written as

$$Y_2O_3 \rightarrow 2Y'_{Zr} + V''_o + 3O_o^{\times} \quad (1)$$

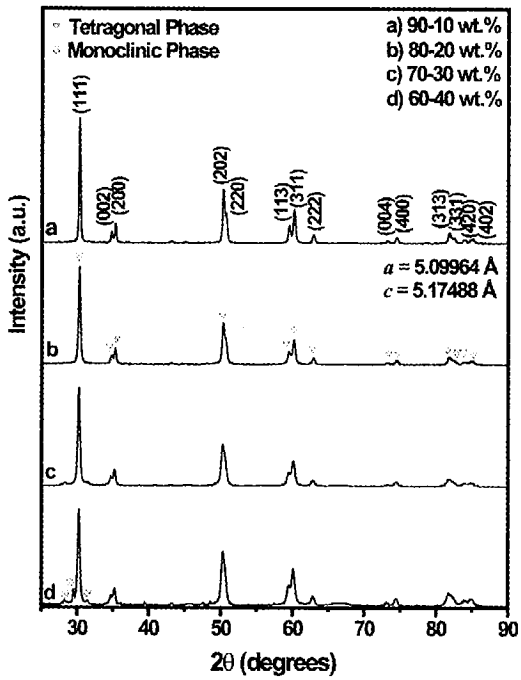

Fig. 2. XRD patterns of *t*-YSZ/Al_2O_3 products, sintered at 1100 °C for 15 h.

and

$$Al_2O_3 \rightarrow 2Al'_{Zr} + V''_o + 3O_o^{\times} \quad (2)$$

In the second series, *c*-YSZ/Al_2O_3, i.e., (8% mol YSZ)/Al_2O_3, cubic fluorite reflections were identified by XRD, in this case zirconia's pure cubic structure was present in all compounds. However, the compound 90/10 exhibited an XRD pattern with the most intense and defined diffracted peaks. In this case, no Al_2O_3 diffraction peaks were observed just a defined lattice with unit cell $a = 0.513921$ Å and space group $Fm\bar{3}m$. A study of the crystal growth with temperature and sintering time was carried out. Figure 3 shows how an increase in the sintering time and temperature affect the peak widths and particle size.

3.2. Micro-Structural Analysis

Studies by SEM of *t*-YSZ/Al_2O_3 and *c*-YSZ/Al_2O_3, which were carried out at high magnification range 50 000X to 250 000X, showed an uniform morphology and homogenous distribution of particles with a size in the range 30–100 nm, Figures 4a and 4b. Semi-spherical clusters were analysed by EDS indicating that there were atomic percent concentrations of alumina which were in good agreement with the starting amounts added to the compounds, Figure 4c.

3.3. AFM Surface Analysis

The morphology and size of the *t*-YSZ–Al_2O_3 and *c*-YSZ–Al_2O_3 sintered particles were analysed by AFM, also the

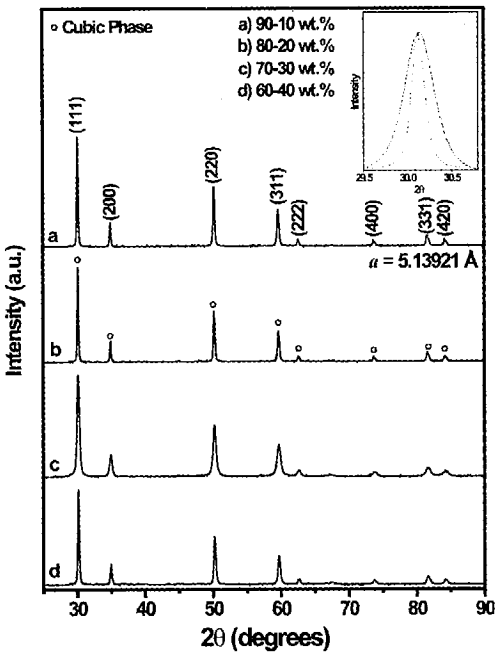

Fig. 3. XRD patterns of c-YSZ/Al_2O_3 products, which were sintered at 1100 °C for 15 h. The crystal growth, through the width change of the most intense peak, for this heat treatment is shown in the inset.

perfilometry of these samples was determined. Agglomerates built of semispherical and spherical nanoparticles were observed.

For those samples which were sintered at 800, 900, 1000, and 1100 °C for 2 and 6 h, the agglomeration of nanoparticles was increased, in most of the scanned zones. On the other hand, pellets which were sintered at 1100 °C for 15 h, revealed a linear array of nanoparticles, this can be associated to the diffusion of nanoparticles with temperature and sintering time. Small differences between

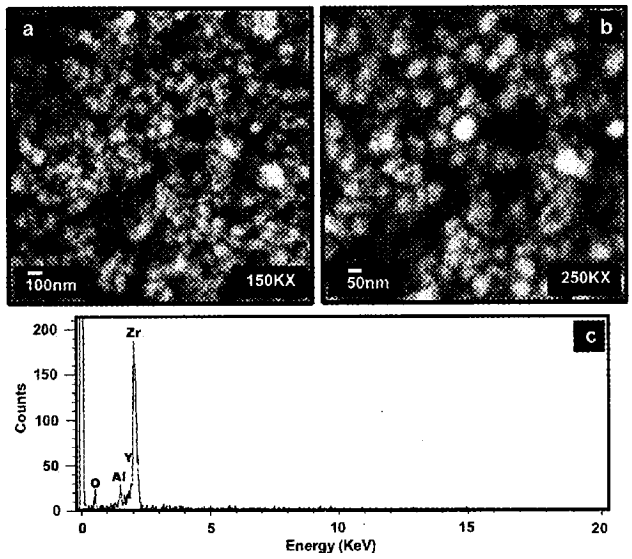

Fig. 4. SEM micrographs, (a) 150 000X and (b) 250 000X, and (c) EDS spectrum of the elemental analysis of the compound.

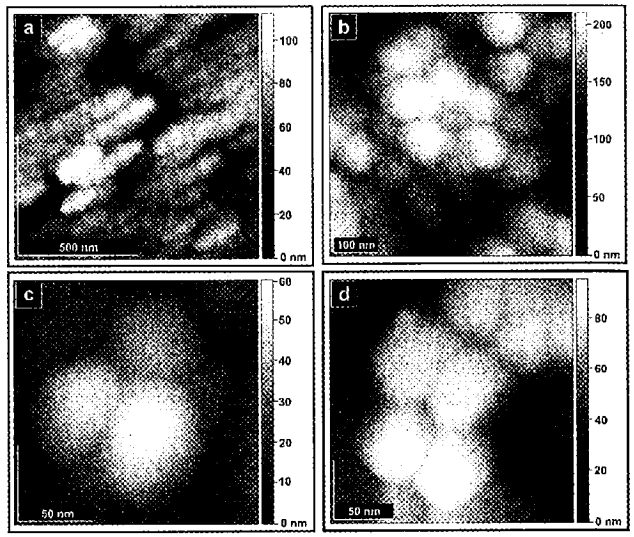

Fig. 5. AFM tapping analyses of samples which were sintered at 1100 °C for 15 h. t-YSZ/Al_2O_3 micrographs for (a) 80/20 wt%, showing linear arrays of grains and (b) 90/10 wt% sample. c-YSZ/Al_2O_3 images with (c) 80/20 wt% and (d) 90/10 wt% compounds.

t-YSZ/Al_2O_3 and c-YSZ/Al_2O_3 were observed in the tapping mode, for both cases images showed particle sizes in the range 30–100 nm with an homogeneous distribution. Profile measurements indicated height differences around ~30 nm for t-YSZ/Al_2O_3. In the c-YSZ/Al_2O_3 case, particle sizes were about 20–100 nm with a smaller sample roughness than that of the t-YSZ/Al_2O_3 sample.

Figure 5a shows a typical micrograph of linear arrays of particles. Figure 5b shows a t-YSZ/Al_2O_3 with 80/20 and 90/10 wt% which was sintered at 1100 °C for 15 h, whilst Figures 5c and 5d show nanoparticles of c-YSZ/Al_2O_3 with 80/20 and 90/10 proportions, respectively. From micrographs (Figs. 5b to 5d), it can be observed that the size distribution and also the particle aggregation are quite similar for all these samples.

Although X-ray diffraction patterns shows that the γ-Al_2O_3 proportion increases until the formation of crystalline structures with lower symmetry; the surface analysis did not show important morphological differences for these samples; homogeneous YSZ/Al_2O_3 nanocompouds were observed, however t-YSZ/Al_2O_3, c-YSZ/Al_2O_3 in proportions of 80/20 wt% and 90/10 wt% for of the γ-Al_2O_3 is related for growing of nanoparticles with linear array.

3.4. TEM and HRTEM Structural and Morphological Results

t-YSZ/Al_2O_3 and c-YSZ/Al_2O_3 nanoparticles were studied by TEM. From these analyses it was possible to identify clusters of 50–100 nm which were formed by nanoparticles in a range 3–10 nm, which are agglomerated within a semi-spherical profile, Figure 6.

The agglomeration of particles was observed in samples which were sintered at 1000 and 1100 °C; however, the

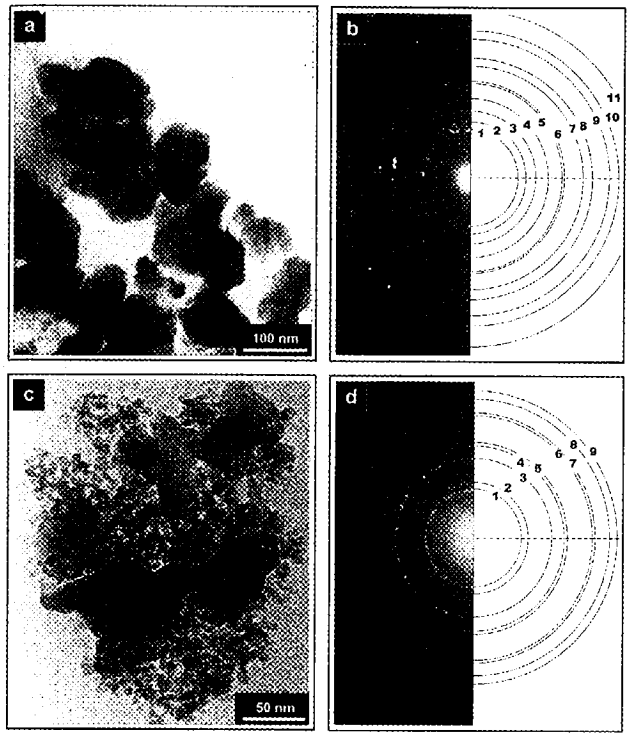

Fig. 6. (a) Micrograph of t-YSZ/Al_2O_3 90/10, (b) its electron diffraction pattern, (c) Micrograph of c-YSZ/Al_2O_3 90/10, and (d) its electron diffraction pattern.

particle size was controlled by a slow increase in the sintering temperature. Figure 6a shows a TEM micrograph of t-YSZ/Al_2O_3 90/10 phase and Figure 6c shows a c-YSZ/Al_2O_3 90/10 product.

Selected area electron diffraction pattern (SAD) showed characteristic discontinuous rings produced by polycrystalline materials with nanometric particle size. Patterns were indexed and for the t-YSZ/Al_2O_3 90/10 phase, Figure 6b, circles have the following correspondence (1) 111, (2) 002, (3) 200, (4) 202, (5) 113, (6) 222, (7) 004, (8) 400, (9) 313, (10) 402, and (11) 224; for the c-YSZ/Al_2O_3 90/10 sample, Figure 6c, the relation is (1) 111, (2) 200, (3) 220, (4) 311, (5) 222, (6) 400, (7) 331, (8) 420, and (9) 422. These results were compared with XRD-Rietveld refinement for the new t-YSZ/Al_2O_3 90/10 phase and JCPDS (Power Diffraction Data, PDF-2 Release 2004) XRD matching well reported zirconia phases for c-YSZ/Al_2O_3 90/10.

Micrographs of t-YSZ/Al_2O_3 80/20 sample of a selected area analysis by using bright field and HAADF images are shown in Figures 7b and 7c, respectively. The use of HAADF contrast, which is directly related to the high angle scattering and to Z (atomic number), allows to identify that clusters are formed by smaller particles with a smooth contrast on the surface, which has been related usually with a core–shell configuration in nanostructures, so it apparently denotes a distribution of nanoparticles with coated surfaces.[34]

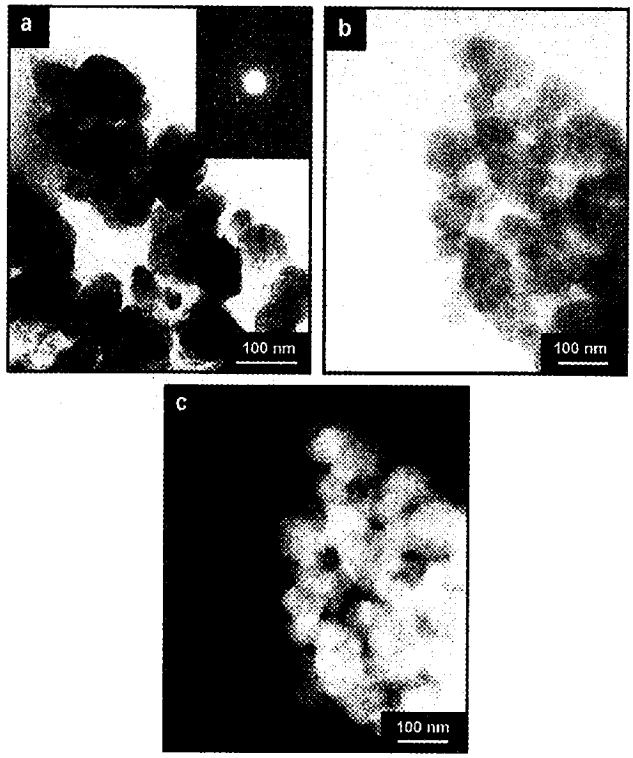

Fig. 7. TEM analyses of samples which were sintered at 1100 °C for 15 h. (a) Aggregation of nanoparticles and electron diffraction pattern (inset) of t-YSZ/Al_2O_3 90/10 sample. Selected area analyses by (b) bright field and (c) HAADF contrast images for t-YSZ/Al_2O_3 80/20 sample.

High resolution TEM was used to evaluate the surface of the powders. An analysis of the internal structure of the particles was obtained, Figure 8, which correspond to HRTEM contrast from the centre of one of the observed

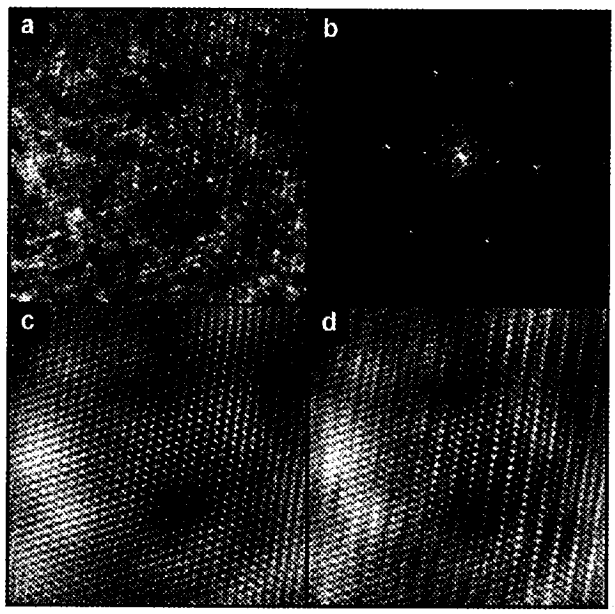

Fig. 8. HRTEM structural analysis of the nanoparticles core. (a) Original image, (b) FFT, and digitally processed images by (c) lattice, and (d) radial filters in the frequencies space.

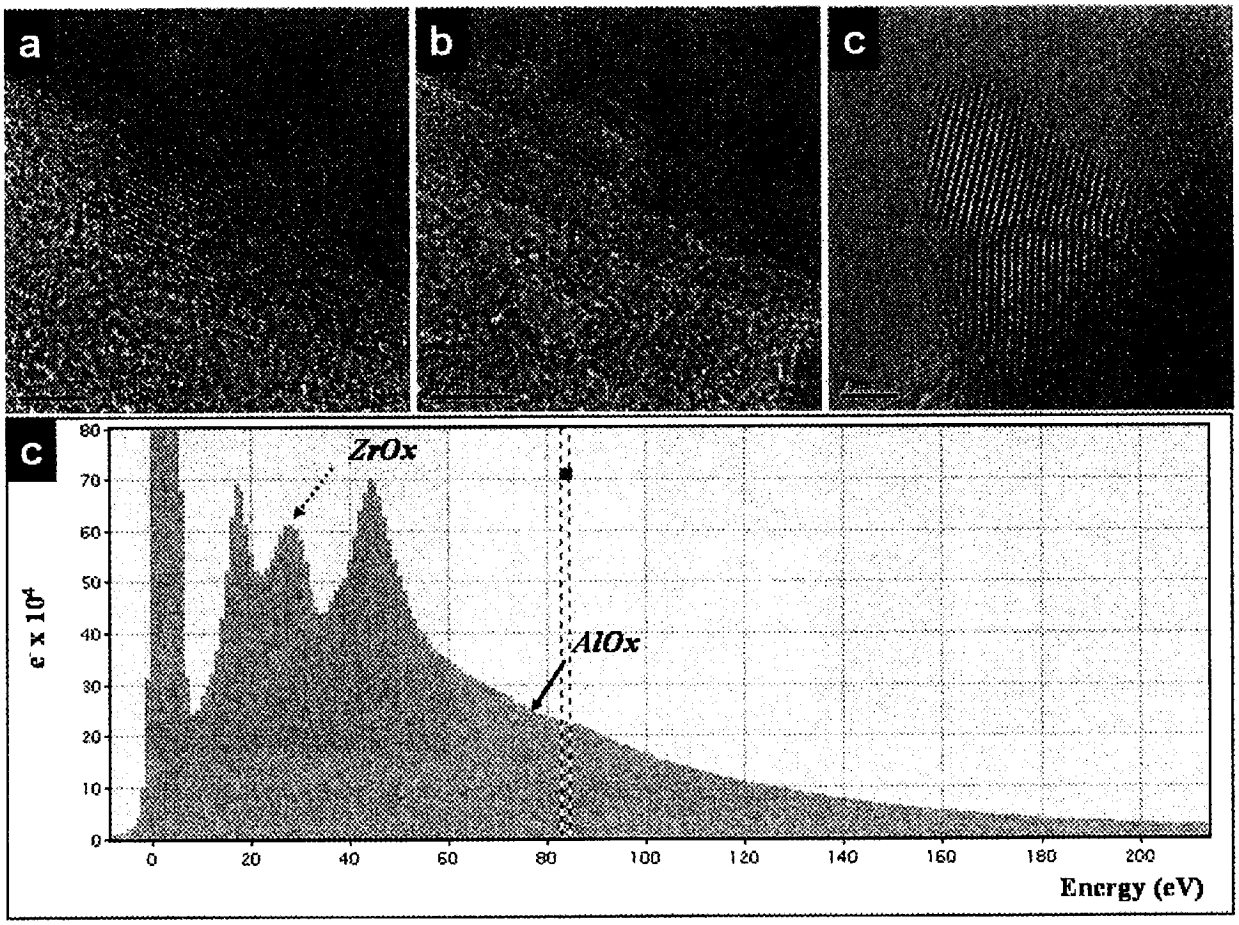

Fig. 9. HRTEM micrographs of t-YSZ/Al_2O_3 with (a) 80/20. (b) 70/30, (c) 60/40 proportions, and (d) EELS spectrum for the t-YSZ/Al_2O_3 with 80/20 sample.

clusters of the sample which was mentioned in Figure 7b. The structural analysis involved the use of an original image, with its corresponding fast Fourier transform (FFT) to identify its periodicity, Figures 8a and 8b, respectively, and a couple of filtered images, based on the use of a selective lattice and radial masks, Figures 8c and 8d, respectively. The use of the processed images and the FFT allowed to determine that the particle is a single phase product of t-YSZ structure observed at the {011} zone axis and with a perfect core and small lattice deformations at the borders. The type of digital filter allowed enhancing the structure using the lattice filter mask, or increases the details of the strain and low dimension distortion reducing the contribution of low frequencies by using an annular mask. This particular contrast was observed in multiple particles of the sample, which may be associated to single crystal clusters that were originally obtained before the addition of the Al_2O_3, however the boundaries and the surface of the particles show distortions and clearly an influence of a different lattice.

In order to determine how the Al_2O_3 is present in the samples and how the distortion on the surface is, the use of HRTEM contrast at higher magnifications and fundamental evaluation of surface of the particles was carried out. In Figure 9, a sequence of micrographs shows the presence and influence of the addition of Al_2O_3 to the system, particularly to the clusters surface as it can be considered from the HAADF analysis.

Three different samples, t-YSZ/Al_2O_3 with 80/20, 70/30, and 60/40 compositions, were evaluated searching for any evidence about the formation of Al_2O_3 crystals. HRTEM micrographs show that there is a layer formation on the YSZ crystal surfaces and the increase of the Al_2O_3 content induces long completed layers, since the continuous layer for the 80/20 sample (low alumina content), Figure 9a, to a well coated surface 60/40 sample (high alumina content), Figure 9c. Also, there is an evidence of irregular surfaces formation with bigger clusters of Al_2O_3 built by rounded aggregates of particles with size in the range 2–3 nm, which emerge from the produced layer generating a higher roughness on the clusters surface.

To demonstrate that the observed crystal has the proposed composition, an EELS spectrum for the t-YSZ/Al_2O_3 with 80/20 sample was obtained. These results, Figure 9d, show two signals which correspond to a high concentration of YSZ and a small contribution of AlO_x.

Results indicate that the formation of an Al_2O_3 layer is made gradually and depending on the increasing of the presence of Al_2O_3 on 70/30 and 60/40 samples. YSZ/Al_2O_3 samples with proportion 80/20 show the formation of small islands on the YSZ surface. Those with 70/30 and 60/40 proportions show a coating of the whole surface of YSZ. For the last sample, a non-homogeneous surface coating formation inducing the production of small clusters, due to the Al_2O_3 excess, must directly affect the functional properties of the material.

4. CONCLUSIONS

In this work, (3 mol% YSZ)/Al_2O_3 and (8 mol%)/Al_2O_3 with proportions 90/10, 80/20, 70/30, and 60/40 were synthesised by co-precipitation to obtain two series of tetragonal and cubic yttria-stabilised-zirconia based phases, i.e., *t*-YSZ 90/10, 80/20, 70/30, and 60/40 and *c*-YSZ 90/10, 80/20, 70/30, and 60/40 phases, respectively. For the (3 mol% YSZ)/Al_2O_3 90/10 product, a novel *t*-YSZ phase was obtained. The structural evolution and influence of nanoparticle size and the Al_2O_3 concentration were studied.

High Al_2O_3 concentrations may introduce unstable structure, for those structures with proportions 30–40 wt% of Al_2O_3 in 3 mol% YSZ the presence of a monoclinic phase is observed mixed with the tetragonal host structure *t*-YSZ. By the addition of 10–20 wt% Al_2O_3 a single tetragonal *t*-YSZ phase was found. Also the sintering temperature and time exposure are important to consolidate nanoparticles in a range from 50–100 nm. Best results were obtained at conditions of 1100 °C during 15 h, where defined polycrystalline phases and homogeneous nanocompounds were got. On other conditions less at 1100 °C during 15 h, i.e., 800–1000 °C for 2 and 6 h, the structures were not good defined. However, the size particle was smaller than the 1100 °C during 15 h in a range 30–80 nm.

Microstructural analyses had shown a linear grown of nanoparticles, this formation could improve some properties of *t*-YSZ and *c*-YSZ materials like structural stability at high temperature, avoiding the phase transformations which decrease the ionic conductivity and deteriorating the mechanical properties. Although, HRTEM, selected area let to identify that the excess of Al_2O_3 induces the formation of a coating layer in samples of YSZ/Al_2O_3 with (a) 80/20, (b) 70/30, and (c) 60/40, it is evident that reduced proportions of Al_2O_3 (less than 10 wt%) form a homogeneous nanocompound.

Acknowledgments: J. Santoyo-Salazar has special thankfulness to CONACYT, DGEP–UNAM, and PAEP–UNAM by Ph.D. Fellowship. Authors express their gratitude to Leticia Baños–López and Carlos Flores–Morales, IIM–UNAM and Luis Rendon, LACMIF–IFUNAM, for technical support.

References and Notes

1. F. Boulc'h, L. Dessemond, and E. Djurado, *Solid State Ionics* 154, 143 (**2002**).
2. A. J. Feighry and J. T. S. Irvine, *Solid State Ionics* 121, 209 (**1999**).
3. M. Dokiya, *Solid State Ionics* 152–153, 383 (**2002**).
4. J. Drennan and G. Auchterlonie, *Solid State Ionics* 134, 75 (**2000**).
5. Y. Wu, A. Bandyopadhyay, and S. Bose, *Mater. Sci. Eng. A* 380, 349 (**2004**).
6. P. S. Badwal, F. T. Ciacchi, and K. M. Giampietro, *Solid State Ionics* (**2004**), in press.
7. S. Tekeli, M. Erdogan, and B. Aktas, *Mater. Sci. Eng.* (**2004**), in press.
8. Y. Wen Zhang, Z. M. Tang, X. Jin, C. Sheng L., and C. Hua Y., *Solid State Sci.* 5, 435 (**2003**).
9. Y. Wu, A. Bandyopadhyay, and S. Bose, *Mater. Sci. Eng. A* 380, 349 (**2004**).
10. R. N. Viwanath and S. Ramasamy, *J. Mater. Sci.* 34, 2879 (**1999**).
11. L. J. M. J. Blomen and M. N. Mugerwa, Fuel Cells Systems, Plenum Press (**1993**), p. 473, 474.
12. J. Kondoh, S. Kikuchi, Y. Tomii, and Y. Ito, *Physica B* 177, 262 (**1999**).
13. E. Torres-Garcia, G. Canizal, S. Velumani, L. F. Ramirez-Verduzco, F. Murrieta-Guevara, and J. A. Ascencio, *Appl. Phys. Mater. A Sci. Process.* 79, 2037 (**2004**).
14. E. Torres-Garcia, G. Rosas, J. A. Ascencio, E. Haro-Poniatowski, and R. Perez, *Appl. Phys. Mater. A Sci. Process.* 79, 401 (**2004**).
15. J. Drennan and G. Auchterlonie, *Solid State Ionics* 134, 75 (**2000**).
16. S. P. S. Badwal, F. T. Ciacchi, and K. M. Giampietro, *Solid State Ionics* (**2004**), in press.
17. A. N. Makareko, A. G. Belous, and Y. V. Pashkova, *J. Euro. Ceramic Soc.* 19, 945 (**1999**).
18. D. Z. de Florio and R. Muccillo, *Solid State Ionics* 123, 301 (**1999**).
19. S. Kikkawa, A. Kijima, K. Hirota, and O. Yamaguchi, *Solid State Ionics* 151, 359 (**2002**).
20. J. C. M'Peko, D. L. Spavieri, Jr., C. L. da Silva, C. A. Fortulan, D. P. F. de Souza, and M. F. Souza, *Solid State Ionics* 156, 59 (**2003**).
21. W. M. Zeng, L. Gao, and J. K. Guo, *Nanostruct. Mater.* 10, 543 (**1998**).
22. E. C. Lu and E. Iglesia, *J. Mater. Sci.* 36, 77 (**2001**).
23. C. H. Laberty-Robert, F. Ansart, C. Deloget, M. Gaudon, and A. Rousset, *Mater. Res. Bull.* 36, 2083 (**2001**).
24. P. Duran, M. Villegas, J. F. Fernandez, F. Capel, and C. Moure, *Mater. Sci. Eng. A* 232, 168 (**1997**).
25. T. P. Raming, A. J. A. Winnubst, W. E. van Zyl, and H. Verweij, *J. Euro. Ceramic Soc.* 23, 1053 (**2003**).
26. F. Ishizaka, T. Yoshida, and S. Sakurada, *Proc. Int. Symp. SOFCs*, edited by O. Yamamoto, M. Dokiya, and H. Tagawa, Nagoya, Japan (**1989**), p. 172.
27. F. J. Esper, K. H. Friese, and H. Geier, *Science and Technology of Zirconia*, edited by N. Claussen, M. Ruhle, and A. H. Heuer, American Ceramic Society, Columbus, OH (**1984**), p. 528.
28. F. Ishizaki, T. Yoshida, and S. Sakurada, *Proc. Electrochem. Soc. Fall Meeting* (**1989**), p. 3.
29. M. H. Kwon, G. H. Kim, H. S. Song, and H. L. Lee, *Mater. Sci. Eng. A* 299, 185 (**2001**).
30. S. Velumani and J. A. Ascencio, *Appl. Phys. Mater. A: Sci. Process.* 79, 153 (**2004**).
31. J. Rodriguez-Carvajal, Computer Program FullProf, Version 3.51, Laboratoire Leon Brillouin. CEA, CNRS, Grenoble, France (**1998**).
32. M. Jose-Yacaman, J. A. Ascencio, S. Tehuacanero, and M. Marin, *Topics in Catalysis* 18, 167 (**2002**).
33. U. Pal, P. Santiago, J. Chavez, and J. A. Ascencio, *J. Nanosci. Nanotechnol.* 5, 609 (**2005**).

Received: 13 January 2006. Revised/Accepted: 17 March 2006.